Structural Eng. / Earthquake Eng. Vol. 7. No. 1, 151s-158s. April 1990
Japan Society of Civil Engineers (Proc. of JSCE No. 416/I-13)

A FIRST ESTIMATION OF RESOLVING POWER OF STRONG-MOTION ARRAY TO INFER HISTORY OF SLIP ON UNIDENTIFIED EARTHQUAKE FAULT

*By Masahiro IIDA**

Resolving power of a strong-motion array for inferring the history of slip on an unidentified earthquake fault is defined as the accuracy of a source inversion.

The accuracy of the source inversion is efficiently calculated using a scheme constructed on the basis of Wolberg's prediction analysis. The resolving power of arrays for identified faults is also estimated to gain an appreciation for unidentified events. We find that the resolving power of the array is gradually enhanced as the station density increases on a square-grid array surrounding an inland fault. Effects of ocean bottom stations deployed for an offshore fault are recognized.

Keywords : strong-motion array, resolving power, accuracy of source inversion, unidentified fault

1. INTRODUCTION

The present study evaluates resolving power of a strong-motion array to infer the history of slip on an unidentified earthquake fault in location and mechanism. In previous studies[1)~3)], resolving power of a strong-motion array for an identified fault was successfully evaluated. More importantly, however, there are few exceptional areas where an earthquake occurrence on a specific fault is expected with a high probability in the short run and intense installation of strong-motion instruments for the fault has been implemented in advance. For example, the majority of recent large earthquakes such as the 1984 Naganoken-Seibu earthquake and the 1983 Nihonkai-Chubu earthquake occurred on ill-prepared condition of strong-motion stations.

Reasonable deployment of strong-motion arrays is required mainly for two reasons. First, inversion studies for estimating various source-structure parameters using array seismograms are neccesitated to predict surface ground motions. Besides, the accuracy of inversion solutions needs be examined to settle large inconsistencies often recognized among the results in current inversion studies. This is also helpful in defining the limitations of inversion studies. Secondly, a guideline for future installation of strong-motion arrays should be prepared. At the 1978 International Workshop on Strong-Motion Earthquake Instrument Arrays[4)], desirable array configurations for typical faults were presented on the basis of intuition. In such situations, a quantitative estimation of resolving power of a strong-motion array is greatly encouraged. Thus far, however, no attempts have been made in a quantitative framework.

We defined the resolving power of a strong-motion array as the accuracy of an inversion solution, which is calculated using the suite of theoretical array seismograms. We concentrated on source effects and

* Member of JSCE, Dr. Eng., Research Associate, Earthquake Research Institute, University of Tokyo (Bunkyo-ku, Tokyo)
Present address : United States Geological Survey (Pasadena, California, USA)

developed a scheme[5] in which the accuracy of a source inversion solution is efficiently calculated on the basis of Wolberg's prediction analysis[6]. Only the far-fiels S waves in a homogeneous full-space are used in that they produce most large amplitudes in acceleration time series and the partial derivatives closely associated with the evaluation of the accuracy of the inversion solution, which would otherwise require additional numerous calculations, are analytically obtained. Theoretical waveform is calculated for a point source located at each center of subdivided fault elements, so that the far-field approximation should be hold for almost all source-receiver combinations. Although only the far-field S waves in a homogeneous full-space are used as a first step, its scheme suggests that more general wave fields and inhomogeneous media can be incorporated. Furthermore, our results may vary with the frequency range of engineering interest, but we do not refer to the general dependence on the frequency without more rigorous and systematic experiments. The target frequency we are here concerned with is constrained by only the size of subfault elements divided.

It permitted us to obtain relationships between the accuracy of the inversion solution and fault-array parameters[1]. An optimum array geometry for the source inversion was determined for each of three types of earthquake faults[2], and was compared with the one proposed on the basis of intuition at the 1978 International Workshop[4]. Resolving power of three existing specific arrays was also explored[3]. All these studies were directed at an identified fault. We should note, however, virtually there are few exceptional areas where a satisfactory array is prepared for an identified, potential fault on which an earthquake is likely to occur for the short term. Nothing has been mentioned on resolving power of an array installed for an unidentified fault in spite of the greater importance.

The present study provides an estimate for effects of the number of array stations, in other words, the station density or the station interval for an unidentified fault. Inland and offshore faults are used. A comparison of the effects for an unidentified fault with those for an identified one will help us to have much understanding of array resolving power.

2. METHOD

Basically, the method used here is the same as was used for an identified fault. As the statistically based method was explained in a greater detail in a previous paper[5], a rough explanation is given here. The accuracy of the solution of a waveform inversion is calculated through errors contained in data by using a principle of error propagation. This is characterized by solving normal equations once without an iterative procedure in an overdetermined least-squares problem.

Since we treat the time behavior of slip on a fault, we divide the fault into N_e subfault elements, and assume that the j-th element starts to slip at a time, t_0^j and release a seismic moment, m_j. For the far-field S wave in a homogeneous full-space, the theoretical displacement amplitude of a time, t_i at the z-th station is formulated as[5]

$$u^z(t_i)=\sum_{j=1}^{N_e}\frac{R^{jz}\cdot m_j\cdot s_j(t_i-r_{jz}/\beta-t_0^j)}{4\pi\rho\beta^3 r_{jz}} \quad \cdots\cdots (1).$$

We denote by R^{jz} and r_{jz}, the radiation pattern of the S wave and the distance from the j-th element to the z-th station, respectively, and also by ρ and β, the density and the S-wave velocity, respectively. A common function is assumed for the source-time function, $s_j(t_i)$ of each subfault, which duration is dependent on the elemental size. The attenuation is treated by assuming an amplitude decay factor of exp $(-\alpha r_{jz})$. The constant, α corresponds to the quality factor, Q and the typical value of Q is empirically assigned (Table 1).

The theoretical amplitude is a function of both unknown and known parameters. Denoting by a_k ($k=1$, $\cdots\cdots$, p) and x_l ($l=1$, $\cdots\cdots$, q), unknown and known parameters, respectively, the theoretical amplitude of the i-th time point at the z-th station can be expressed as $f_i^z(x_{1zi},\cdots\cdots,x_{qzi};\ a_1,\cdots\cdots a_p)$. Unknown

parameters are the seismic moment, m_j and the rupture onset time, t_0^j for each element. Normally distributed errors are independently assumed for known parameters : the strike direction, the dip angle, and the slip angle of each subfault, and for the theoretical amplitude and the arrival time. We define two residuals as the differences between the observed and theoretical values,

$$\left.\begin{aligned} R_{zi}&=F_i^z-f_i^z \\ R_{lzi}&=X_{lzi}-x_{lzi} \end{aligned}\right\} \quad \cdots\cdots (2),$$

where F_i^z and X_{lzi} indicate the observed amplitude and the true value of the l-th parameter of the i-th time point at the z-th station, respectively. We seek a solution which minimizes the weighted sum of the squares of the two kinds of residuals,

$$S=\sum_z\sum_i (w_{zi}R_{zi}^2+\sum_l w_{lzi}R_{lzi}^2) \quad \cdots\cdots (3).$$

Weights, w_{zi} and w_{lzi} are defined as the reciprocals of the variances. Defining δ as a small variation, from the minimization,

$$\delta S=0 \quad \cdots\cdots (4).$$

Normal equations which are written in a matrix form can be obtained,

$$C\cdot A=B \quad \cdots\cdots (5),$$

where an element of the matrix of A, A_k indicates the difference between the value of the unknown parameter, a_k, and its initial guess, a_{k0}, i. e., $A_k=a_{k0}-a_k$. An element of the matrices, B and C is expressed as follows,

$$B_k=\sum_z\sum_i \frac{\partial R_{zi}}{\partial a_k}\cdot\frac{R_{zi0}}{L_{zi}}$$

$$C_{mn}=\sum_z\sum_i \frac{\partial R_{zi}}{\partial a_m}\cdot\frac{\partial R_{zi}}{\partial a_n}\Big/ L_{zi}$$

where

$$L_{zi}=\frac{\left(\dfrac{\partial R_{zi}}{\partial f_i^z}\right)^2}{W_{zi}}+\sum_l \frac{\left(\dfrac{\partial R_{zi}}{\partial x_{lzi}}\right)^2}{W_{lzi}}$$

$$R_{zi0}=F_i^z-f_i^z(X_{1zi},\ \cdots\cdots,\ X_{qzi};\ a_{10},\ \cdots\cdots,\ a_{p0}).$$

Following Wolberg[6], the uncertainty of the k-th unknown parameter, σ_{a_k} can be estimated without solving the normal equations, but by calculating an inverse matrix of the matrix, C.

$$\sigma_{a_k}^2=C_{kk}^{-1} \quad \cdots\cdots (7).$$

This technique called "prediction analysis" is much more advantageous than a Monte Carlo simulation because the equations need only be solved once for each set of array station locations and rupture mode on the target fault. The maximum standard deviation of errors, $\sigma=\max(\sigma_{a_k}/m_k)$ in estimating the seismic moment for each subfault element, which is normalized by the assumed seismic moment, is chosen as the accuracy of the source inversion, i. e., the resolving power because errors in estimating the rupture onset time turn out to be underestimated and less reliable. A single parameter is the best in an attempt to estimate the resolving power of an array, and the choice of σ as the parameter is primarilly reasonable in terms of recent source parameterization[7),8)] and inferring a reliable image of the time behavior of slip over the whole fault.

3. NUMERICAL EXPERIMENT

Fault-array layouts used are depicted in Fig. 1. Two types of earthquake faults are an inland fault and an offshore one. The rupture is assumed to propagate unilaterally with a constant rupture velocity. Parameters assumed for the earthquake faults are summarized in Table 1. The position of the center of the fault falls within the shaded rectangular zone by an uniform random number. In the case of the inland fault, a pure strike-slip fault or a pure dip-slip fault is supposed to be expected with the same probability. In the

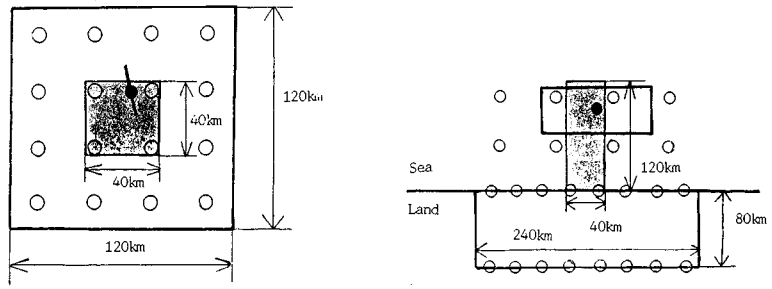

(1) inland fault (2) offshore fault

Fig. 1 Fault-array layouts used. Two types of earthquake faults are an inland fault and an offshore one. The position (indicated by a solid circle) of the center of the fault (a bar or a rectangle) falls within the shaded rectangular zone by an uniform random number. In the case of the inland fault, a pure strike-slip fault or a pure dip-slip fault is supposed to be expected with the same probability, and an array of stations (open circles) arranged in a square-grid form is used. In the case of the offshore fault, only a thrust fault is utilized, and the same land array geometry is adopted regardless of the presence of ocean bottom stations (OBSs). An array of land stations arranged along two lines, the shoreline and another line parallel to the shoreline, is adopted. Effects of OBSs are tested in some cases for the offshore fault. In the both types of faults, the number of stations (the station interval) is varied. An example of fault-array layout is shown for each fault type. See text for a more comprehensive explanation.

Table 1 Parameters assumed for the earthquake faults.

	Inland fault	Offshore fault
Fault area, A_f	30 km×10 km	120 km×60 km
Number of elements, N_e	12	18
Subfault area, A_s	5 km×5 km	20 km×20 km
Strike direction, ϕ	free	parallel to shoreline
Slip direction, λ	pure strike slip or pure dip slip	pure dip slip (thrust)
Dip angle, δ	90° (strike slip) or 30° (dip slip)	30°
Final offset, D	1.0 m	4.0 m
Rise time, τ	6.0 s	16.9 s
Rupture mode	unilateral	unilateral
Rupture velocity, V_r	2.5 km/s	2.5 km/s
Depth of fault center, h	7 km	25 km
S-wave velocity, V_s	3.5 km/s	3.5 km/s
Density of medium, ρ	3.0 t/m^3	3.0 t/m^3
Quality factor, Q	300.0	300.0

case of the offshore fault, only a thrust fault is utilized and effects of strong-motion ocean bottom stations are tested in some cases. Also, as it has been proved that the accuracy of the source inversion, σ is affected by the distance between the fault center and the shoreline, ΔD, its influence is assesed.

In the case of the inland fault, an array of stations arranged in a square-grid form is used because an equal station interval may be convinient. The number of stations, in other words, the station density or the station interval is varied, and the effects on the accuracy of the inversion solution are evaluated. Four cases examined are (1) the number of stations, N_s=9 (the station interval, Δd=40 km), (2) N_s=16 (Δd=30 km), (3) N_s=36 (Δd=20 km), and (4) N_s=64 (Δd=15 km). In the case of the offshore fault, the same land array geometry is adopted regardless of the presence of ocean bottom stations (OBSs). Land stations are arranged along two lines, the shoreline and another line parallel to the shoreline because we realize its advantage through a priori simulations. The interval between the two lines is 80 km, which is determined by a few simulations. The number of stations (the station interval) is varied, and the effects on

the accuracy of the inversion solution are evaluated for two conditions without and with OBSs. Four cases without OBSs conducted are (1) N_s=12 (Δd=40 km), (2) N_s=16 (Δd=30 km), (3) N_s=24 (Δd=20 km), and (4) N_s=32 (Δd=15 km). Other four cases with OBSs conducted are (1) N_s=12 (Δd=40 km) and the number of ocean bottom stations, N_o=6, (2) N_s=16 (Δd=30 km) and N_o=8, (3) N_s=24 (Δd=20 km) and N_o=12, and (4) N_s=32 (Δd=15 km) and N_o=16. An effective installation of OBSs is derived from trial simulations. As a result, in only the case of N_o=6, OBSs are aligned with an equal interval of 40 km along a parallel line to and 80 km away from the shoreline. In the other cases, they are aligned with twice the interval of land stations along two parallel lines to and 50 km and 100 km away from the shoreline.

The accuracy of the inversion solution thus obtained is compared with the one expected if the same earthquake fault is identified in the location and the mechanism. We will choose the same number of stations as the case (2) for each simulation of unidentified faults. Then the most preferable array pattern (station distribution) for each identified fault is used. The array station distribution is determined by a trial and error modeling in accordance with the procedure implemented in a previous study[2]. In simulations of the offshore fault, four values of ΔD (ΔD=15 km, 45 km, 75 km, and 105 km) are taken due to the large dependency of the accuracy of the solution on ΔD.

4. RESULTS AND DISCUSSION

The accuracy of the inversion solution, σ for two types of unidentified faults (inland and offshore) are summarized in Table 2, and the schematic plots of σ are given in Fig. 2. A total of 30 measurements with different faults is performed for each station pattern. We may emphasize a large variation in the accuracy of the inversion solution, σ for an unidentified fault (Fig. 2). In particular, the accuracy becomes rapidly degraded with the considerable diminution in the number of stations in the case of an inland fault (Fig. 2 (a)). Also, it is proved that the accuracy remains gradually improved as the number of stations increases, whereas the accuracy for an identified inland fault was in inverse proportion to the number of stations[1]. Similarly, in the case of an offshore fault (Figs. 2(b) and 2(c)), the accuracy is not remarkably enhanced with the increase in the number of stations. A comparison between Fig. 2(2) and 2(3) reveals an installation effect of OBSs for an unidentified offshore fault. For example, see the case of 24 stations in the total number in both figures.

The accuracy of the inversion solution, σ, which is derived using the most preferable array geometry for each of identified faults, is listed throughout all the cases in Table 3. The preferable geometries are exhibited for most cases in Fig. 3. For comparison, the σ values are also plotted with cross marks in

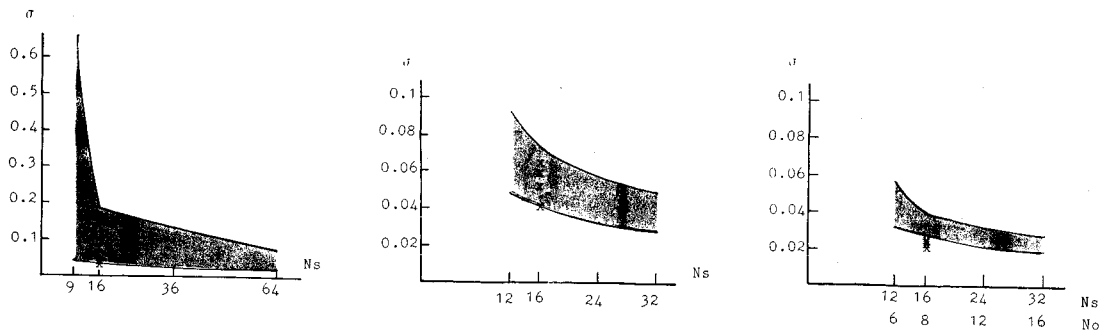

(1) inland fault (2) offshore fault without OBSs (3) offshore fault with OBSs

Fig. 2 Relationship between the accuracy of the inversion solution, σ and the number of land stations, N_s for unidentified faults. In the condition with OBSs for an offshore fault, the number of OBSs, N_o is half N_s. The σ ranges numerically given in Table 2 are displayed by the shaded zone. A cross means the accuracy obtained with the same number of stations for each comparable identified fault.

Table 2 Effects of the number of stations, N_s (or the station interval, Δd) on the accuracy of the inversion solution, σ for unidentified faults : (a) inland and (b) and (c) offshore. Two conditions (b) without and (c) with OBSs are tested for the offshore fault. The minimum, average, and maximum of 30 measurements are shown for each station pattern.

(a) Inland fault

N_s	Δd (km)	σ		
		minimum	average	maximum
9	40	0.047	0.154	0.659
16	30	0.037	0.092	0.191
36	20	0.025	0.055	0.136
64	10	0.019	0.040	0.077

(b) Offshore fault (without OBSs)

N_s	Δd (km)	σ		
		minimum	average	maximum
12	40	0.049	0.073	0.092
16	30	0.041	0.060	0.074
24	20	0.033	0.048	0.058
32	15	0.029	0.041	0.051

(c) Offshore fault (with OBSs)

N_s	N_o	Δd (km)	σ		
			minimum	average	maximum
12	6	40	0.031	0.042	0.057
16	8	30	0.028	0.034	0.040
24	12	20	0.022	0.027	0.032
32	16	15	0.020	0.024	0.028

Table 3 The accuracy of the source inversion, σ derived using the most preferable array geometry for each of identified faults. Two conditions without and with OBSs are tested for the offshore fault. N_s, N_o, and ΔD mean the number of land stations, the number of OBSs, and the distance between the fault center and the shoreline, respectively. Note that four values of ΔD values are taken for the offshore fault.

		σ
(1)	Inland strike-slip fault (N_s=16)	0.031
(2)	Inland dip-slip fault (N_s=16)	0.038
(3)	Offshore fault (N_s=16) ΔD=15 km	0.042
	ΔD=45 km	0.060
	ΔD=75 km	0.065
	ΔD=105 km	0.052
(4)	Offshore fault (N_s=16 and N_o=8) ΔD=15 km	0.024
	ΔD=45 km	0.023
	ΔD=75 km	0.024
	ΔD=105 km	0.022

Table 4 Difference in the accuracy of the inversion solution, σ between unidentified inland strike-slip and dip-slip faults. The results for the 16-station (the 30 km-station-interval) simulation are picked up.

	σ		
	minimum	average	maximum
Strike-Slip	0.068	0.128	0.191
Dip-slip	0.037	0.043	0.051

Fig. 2.

The desired array geometry for an identified strike-slip fault has a different feature from that for a dip-slip event (Result A). By separating the results obtained for the 16-station simulation of unidentified inland faults into two according to the fault type, we also see the distinct difference in the accuracy between strike-slip and dip-slip faults (Result B), as shown in Table 4. The reason for the Result B could be attributed to the dip angle recognized between the two kinds of faults[1] : while the arrivals of seismic waves from subfault elements can be separated in time at distant stations for a dip-slip fault with a dip angle of 30°, they can not be so well separated for a strike-slip fault with a dip angle of 90° that the accuracy becomes worse for the strike-slip fault. Both Results A and B support a view that distant stations are not effective for a strike-slip fault, so that we cannot expect so good an accuracy as for an unidentified strike-slip fault. The accuracy for identified inland faults is good agreement with the highest limit of that for unidentified events. This seems to be very likely.

As for identified offshore faults, we confirm that the desired land array pattern is not changed regardless of the presence of OBSs (Fig. 3). In the presence of OBSs, the accuracy is not so sensitive to the distance, ΔD. Without OBSs, in contrast, the accuracy is controlled by ΔD (Table 3). This implies that unnatural phenomena may be caused that the accuracy for identified offshore faults is occasionally worse than that for unidentified ones owing to the difference in ΔD, as shown in (2) of Fig. 2, when no OBSs are installed. Given several OBSs, the accuracy for identified offshore faults is always better than that for unidentified events.

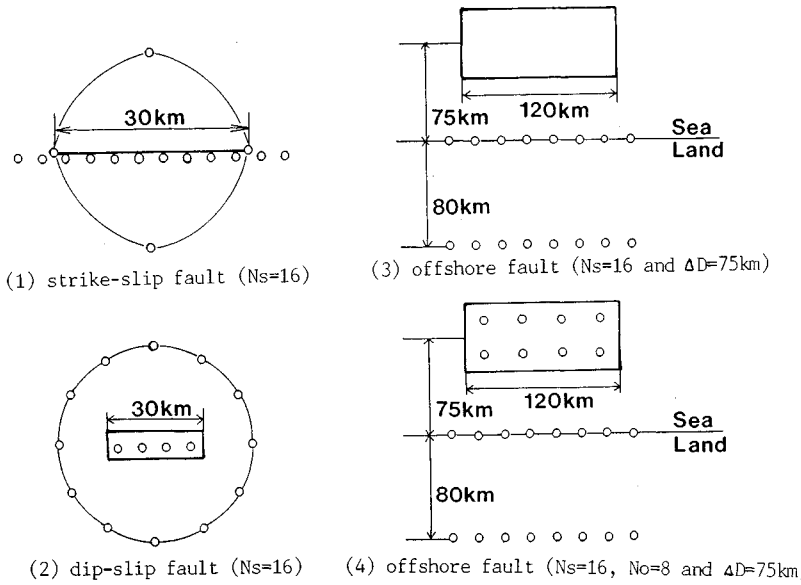

Fig. 3 The most preferable array geometry obtained for each of identified faults. Two conditions without and with OBSs are tested. N_s, N_o, and ΔD mean the number of land stations, the number of OBSs, and the distance between the fault center and the shoreline, respectively. Note that the array geometry is presented only for a single value of ΔD of 75 km for the offshore fault.

5. CONCLUSIONS

Resolving power of a strong-motion array for inferring the history of slip on an unidentified earthquake fault has been defined as the accuracy of a source inversion using the suite of array theoretical seismograms. The accuracy of the source inversion has been efficiently calculated using a scheme constructed on the basis of Wolberg's prediction analysis. We have investigated effects of the number of stations, in other words, the station interval for two types of faults : inland and offshore thrust. For reference, the resolving power of arrays for such unidentified faults has been compared with that for identified events.

We have found that the resolving power of the array is gradually enhanced as the station density increases on a square-grid array surrounding an inland fault. Effects of ocean bottom stations (OBSs) deployed for an offshore fault have been revealed. The accuracy of the inversion solution for identified inland faults grossly corresponds to the highest limit of that for the unidentified events. However, the accuracy for identified offshore faults may be worse than that for the unidentified events when no OBSs are deployed because the accuracy is controlled by the distance between the fault center and the shoreline.

REFERENCES

1) Iida, M., Miyatake, T. and Shimazaki, K. : Relationship between the accuracy on source inversion and source and array parameters, and the interpretation, Proc. 7th Japan Earthq. Eng. Symp., pp. 451-456, 1986.
2) Iida, M., Miyatake, T. and Shimazaki, K. : Optimum strong-motion array geometry for source inversion, Earthq. Eng. Struct. Dyn., Vol. 16, pp. 1213-1225, 1988.
3) Iida, M. : Preliminary estimation of ability to infer earthquake source processes in Japanese strong-motion arrays, Proc. Japan Soc. Civil Eng., Vol. I-10, pp. 147-155, 1988.
4) Iwan, W. D. (Editor) : Strong-motion earthquake instrument arrays, Proc. Int. Workshop Strong-motion earthquake instrument arrays, Honolulu, Hawaii, 1978.

5) Miyatake, T., Iida, M. and Shimazaki, K. : The effects of strong-motion array configuration on source inversion, Bull. Seism. Soc. Am., Vol. 76, pp. 1173-1185, 1986.
6) Wolberg, J. R. : Prediction Analysis, D. Van Nostrand Co. Inc., Princeton, New Jersey, 1967.
7) Beroza, G. C. and Spudich, P. : Linearized inversion for fault rupture behavior : application to the 1984 Morgan Hill, California, earthquake, J. Geophys. Res., Vol. 93 B, 6275-6296, 1988.
8) Hartzell, S. and Iida, M. : Source complexity of the 1987 Whittier Narrows, California, earthquake from the inversion of strong motion records, (submitted to J. Geophys. Res., 1990).

(Received April 18 1989)